International Journal of Solids and Structures 225 (2021) 111067

Contents lists available at ScienceDirect

International Journal of Solids and Structures

journal homepage: www.elsevier.com/locate/ijsolstr

Modeling inelastic spin of microstructural vectors in sheet metal forming

Eun-Ho Lee [a,b], M.B. Rubin [c]

[a] School of Mechanical Engineering, Sungkyunkwan University, Suwon, Gyeonggi-do 16419, Republic of Korea
[b] Department of Smart Fab. Technology, Sungkyunkwan University, Suwon, Gyeonggi-do 16419, Republic of Korea
[c] Faculty of Mechanical Engineering, Technion-Israel Institute of Technology, 32000 Haifa, Israel

ARTICLE INFO

Article history:
Received 20 January 2021
Accepted 19 April 2021
Available online 26 April 2021

Keywords:
Orthotropic inelastic deformation rate
Eulerian formulation
Inelastic spin
Microstructural vectors
Sheet metal forming

ABSTRACT

This paper develops a new functional form for the inelastic spin that influences the orientation of microstructural vectors during large inelastic deformations in a recently developed Eulerian formulation of sheet metal. For the problems under consideration, a single constant determines the inelastic spin, and the results of the New model are compared to those of a common Lagrangian sheet metal model. It is shown that the same value of this constant causes the New model to predict good results relative to measured data for uniaxial stress at angles relative to the RD, equibiaxial stress and the R-value distribution for AA6022-T4 sheet metal. In contrast, the Lagrangian model predicts zero inelastic spin, which is inconsistent with the measured data. The example of large deformation simple shear is used to further examine the influence of inelastic spin predicted by the New model and the Lagrangian model. The results show that the predictions of the New model, which is insensitive to arbitrariness of a reference configuration, are reasonable, while those of the Lagrangian model exhibit an unphysical dependence on the reference configuration.

1. Introduction

Recently, Lee and Rubin (2020) presented the theory and validation of an elastically isotropic, inelastically orthotropic model for sheet metals, which is based on an Eulerian formulation of evolution equations for microstructural vectors $\mathbf{m}_i$ that characterize elastic deformations and material orientations. In a zero-stress state, the microstructural vectors can be initially aligned to the orthotropic axes - rolling direction (RD), transverse direction (*TD*), and thickness axes. The Eulerian evolution equations for $\mathbf{m}_i$ depend on constitutive equations for inelastic deformation rate and inelastic spin. As the material is deformed, the vectors $\mathbf{m}_i$ deform and rotate. Elastic deformations cause $\mathbf{m}_i$ to become a skewed and stretched triad which is used in a hyperelastic constitutive equation to determine the Cauchy stress.

Deformation theory has been widely studied to define inelastic deformation rate (Budiansky, 1959; Hutchinson, 1974; Stören and Rice, 1975; Levy et al., 1978; Chung and Lee, 1984; Sklad, 1986; Batoz et al., 1989; Neale, 1989). The minimum plastic work theory is often employed to define a deformation path (Hill, 1957; Hill, 1986; Nádai and Hodge, 1963; Ponter and Martin, 1972; Chung and Richmond, 1992; Chung and Richmond, 1993; Yoon et al., 1999), and this theory has provided good numerical results in engineering problems (Park et al., 1999; Kim et al., 2000; Kim and Yang, 2007; Lee et al., 2015; Lee et al., 2017). Many of these models employed the standard Lagrangian formulation of plasticity (A et al., 1957; Kröner, 1959; Lee, 1969) that introduces a multiplicative form for elastic deformation as a function of total deformation and plastic deformation. A more recent model (Vladimirov et al., 2010) uses the mulitplicative formulation with structural tensors to characterize anisotropy.

As shown in (Rubin, 1996; Rubin, 2001), the Lagranian formulation contains unphysical arbitrariness of: a reference configuration, a zero-stress intermediate configuration, a measure of total deformation and a measure of inelastic deformation. The Eulerian formulation in (Eckart, 1948; Leonov, 1976) was generalized in (Rubin, 1994) by introducing evolution equations for the microstructural vectors $\mathbf{m}_i$, and it was shown in (Rubin, 2012) that this model removes the aforementioned arbitrariness.

The constitutive equations for inelastic deformation rate and inelastic spin proposed in (Lee and Rubin, 2020) ensure that inelastic deformation rate is dissipative and were calibrated to predict the R-value distribution of sheet metal with respect to the angle of loading from the *RD* for MP980 and AA6022-T4 sheet metals. This Eulerian formulation yields stress components relative to elastic distortional deformation vectors $\mathbf{m}_i'$ which are insensitive to Superposed Rigid Body Motions (*SRBM*) and can be used directly

E-mail addresses: e.h.lee@skku.edu (E.-H. Lee), mbrubin@tx.technion.ac.il (M.B. Rubin)

https://doi.org/10.1016/j.ijsolstr.2021.111067
0020-7683/

in existing anisotropic yield functions (Hill, 1948; Barlat et al., 1991; Barlat et al., 1997; Barlat et al., 2003; Banabic et al., 2005; Hu et al., 2017; Lou and Yoon, 2018; Yoon et al., 1999). Specifically, in (Lee and Rubin, 2020) use was made of the Coupled Quadratic-Nonquadratic (CQN) yield function proposed in (Lee et al., 2017), which was shown to model observed anisotropic evolution of hardening observed for MP980 and AA6022-T4 sheet metals.

Many sheet metal models do not include the effect of inelastic spin (Chung and Richmond, 1992; Chung and Richmond, 1993; Yoon et al., 1999; Kim and Yang, 2007; Lee et al., 2015; Lee et al., 2017). However some papers report that inelastic spin has a significant influence even for uniaxial tension (Dafalias and Rashid, 1989; Kim and Yin, 1997; Bunge and Nielsen, 1997; Dafalias, 1998; Tong et al., 2004). The objective of this paper is to develop a functional form for inelastic spin that is calibrated relative to measured data (Tong et al., 2004) on the rotation of orthotropic axes during uniaxial stress at angles relative to the RD for sheet metal. Predictions of this Eulerian formulation are compared with those of a common Lagrangian formulation based on the rotation tensor in the polar decomposition of the deformation gradient. The results of uniaxial tension examples show that the Eulerian model can be calibrated to predict measured orientation changes in the directions of orthotropy, whereas the predictions of the Lagrangian model are inconsistent with the measured data since it does not model inelastic spin. Predictions of these models are also compared for large simple shear deformation. The results for simple shear show that the Lagrangian model exhibits unphysical dependence on the reference configuration. In contrast, the Eulerian formulation based on the microstructural vectors $\mathbf{m}_i$ predicts reasonable inelastic spin and is insensitive to this arbitrariness.

An outline of the paper is as follows. Section 2 presents a summary of the Eulerian formulation presented in (Rubin, 1994) and the specific constitutive model discussed in (Lee and Rubin, 2020). It also presents a new functional form for the inelastic spin. Section 3 describes the Lagrangian and Eulerian models used for comparison and records the material properties of AA6022-T4 sheet metal used in the example problems. This section also defines orientation angles which are used for comparison of the new and reference models. Section 4 uses measured data of the rotation angle in (Tong et al., 2004) for uniaxial stress at angles relative to the RD to calibrate the new constant $\bar{\Omega}_{12}$ in the inelastic spin function. The calibrated model is shown to predict good results relative to measured data for the strain-strain curves for uniaxial stress at angles relative to the RD and for Equibiaxial stress (EB), as well as the R-value distribution for AA6022-T4 sheet metal. Section 5 studies the influence inelastic spin for large deformation simple shear and Section 6 presents conclusions.

2. Summary of the constitutive model

2.1. Kinematics

A material point is located by the position vector $\mathbf{x}$ at time t and its velocity is defined by

$$\mathbf{v} = \dot{\mathbf{x}}, \tag{1}$$

where a superposed dot $\dot{(\,)}$ denotes material time differentiation. Also, the velocity gradient $\mathbf{L}$, the deformation rate $\mathbf{D}$ and the spin $\mathbf{W}$ are defined by

$$\mathbf{L} = \partial\mathbf{v}/\partial\mathbf{x} = \mathbf{D} + \mathbf{W}, \quad \mathbf{D} = \frac{1}{2}\left(\mathbf{L} + \mathbf{L}^T\right), \quad \mathbf{W} = \frac{1}{2}\left(\mathbf{L} - \mathbf{L}^T\right). \tag{2}$$

2.2. Elastic deformation measures and orthotropic invariants

In (Lee and Rubin, 2020) use was made of the recent work in (Rubin, 2019) for thermomechanical response of orthotropic elastic-inelastic soft materials to develop a model for metal forming. Specifically, in the absence of inelastic dilatational rate, the elastic dilatation J_e satisfies the equations

$$J_e = \frac{\rho_0}{\rho}, \quad \frac{\dot{J}_e}{J_e} = \mathbf{D}\cdot\mathbf{I}, \tag{3}$$

where ρ is the current mass density, ρ_0 is the zero-stress mass density, $\mathbf{A}\cdot\mathbf{B} = \mathrm{tr}\left(\mathbf{A}\mathbf{B}^T\right)$ is the inner product between two second order tensors $\mathbf{A}, \mathbf{B}$ and $\mathbf{I}$ is the second order identity tensor. Also, the distortional elastic microstructural vectors $\mathbf{m}'_i$ $(i = 1, 2, 3)$ are determined by the evolution equations

$$\dot{\mathbf{m}}'_i = \left(\mathbf{L}'' - \Gamma\bar{\mathbf{L}}''_p\right)\mathbf{m}'_i, \quad \bar{\mathbf{D}}_p = \frac{1}{2}\left(\bar{\mathbf{L}}''_p + \bar{\mathbf{L}}''^T_p\right), \quad \bar{\mathbf{W}}_p = \frac{1}{2}\left(\bar{\mathbf{L}}''_p - \bar{\mathbf{L}}''^T_p\right), \tag{4}$$

where $\mathbf{L}''$ is the deviatoric part of $\mathbf{L}$, Γ is a non-negative function that controls the magnitude of inelastic rate, $\bar{\mathbf{L}}''_p$ is a deviatoric tensor that controls the direction of inelastic rate, $\bar{\mathbf{D}}_p$ is a deviatoric tensor that controls the direction of inelastic distortional deformation rate and $\bar{\mathbf{W}}_p$ is a deviatoric tensor that controls the direction of inelastic spin. Alternatively, as briefly discussed in (Lee and Rubin, 2020), functional forms for crystal plasticity can be used to motivate an expression for $\bar{\mathbf{L}}_p$ in terms of the microstructural vectors $\mathbf{m}'_i$.

The elastic distortional deformation metric m'_{ij}, the elastic distortional deformation reciprocal vectors $\mathbf{m}^{i\prime}$ and the elastic distortional deformation reciprocal metric $m^{ij\prime}$ satisfy the equations

$$\begin{aligned} &m'_{ij} = \mathbf{m}'_i\cdot\mathbf{m}'_j, \quad \mathbf{m}'_i\cdot\mathbf{m}^{j\prime} = \delta^j_i, \quad m^{ij\prime} = \mathbf{m}^{i\prime}\cdot\mathbf{m}^{j\prime}, \\ &\dot{m}'_{ij} = \mathbf{M}_{ij}\cdot\left(\mathbf{D} - \Gamma\bar{\mathbf{D}}_p\right), \quad \mathbf{M}_{ij} = \mathbf{m}'_i\otimes\mathbf{m}'_j + \mathbf{m}'_j\otimes\mathbf{m}'_i - \tfrac{2}{3}m'_{ij}\mathbf{I}, \end{aligned} \tag{5}$$

where $\mathbf{a}\otimes\mathbf{b}$ denotes the tensor product between two vectors $\mathbf{a}, \mathbf{b}$ and δ^j_i is the Kronecker delta. Also, for the special case of isotropic elastic response, the orthotropic invariants β_i reduce to

$$\begin{aligned} &\beta_1 = m'_{11} + m^{11\prime}, \beta_2 = m'_{22} + m^{22\prime}, \beta_3 = m'_{33} + m^{33\prime}, \\ &\beta_4 = \tfrac{m^{2\prime}_{12}}{m'_{11}\,m'_{22}}, \beta_5 = \tfrac{m^{2\prime}_{13}}{m'_{11}\,m'_{33}}, \beta_6 = \tfrac{m^{2\prime}_{23}}{m'_{22}\,m'_{33}}, \end{aligned} \tag{6}$$

which satisfy the evolution equations

$$\dot{\beta}_i = 2\mathbf{B}''_i\cdot\left(\mathbf{D} - \Gamma\bar{\mathbf{D}}_p\right), \tag{7}$$

where the deviatoric tensors $\mathbf{B}''_i$ are functions of $\mathbf{m}'_i$ defined in (Rubin, 2019; Lee and Rubin, 2020) and are recorded in A for convenience.

2.3. Constitutive equations

For elastically isotropic isothermal response, the Helmholtz free energy ψ per unit mass was specified in (Lee and Rubin, 2020) by

$$\rho_0\psi = \frac{1}{2}K(J_e - 1)^2 + \frac{\mu}{4}\sum_{i=1}^{3}(\beta_i - 2), \tag{8}$$

where K, μ are the zero-stress bulk and shear modulus, respectively. Also, the associated Cauchy stress $\mathbf{T}$ is given by

$$\mathbf{T} = -p\mathbf{I} + \mathbf{T}'', \quad p = K(1 - J_e), \quad \mathbf{T}'' = \frac{\mu}{2}J_e^{-1}\sum_{i=1}^{3}\mathbf{B}''_i. \tag{9}$$

where p is the pressure and $\mathbf{T}''$ is the deviatoric part of $\mathbf{T}$. Moreover, the components T_{ij} of $\mathbf{T}$ relative to $\mathbf{m}_i'$ are defined by

$$\begin{aligned} T_{ij} &= T_{ij}(J_e, m_{rs}') = \mathbf{T}\cdot\mathbf{m}_i'\otimes\mathbf{m}_j' = -p\,m_{ij}' + T_{ij}'', \\ T_{ij}'' &= \mathbf{T}''\cdot\left(\mathbf{m}_i'\otimes\mathbf{m}_j'\right) = T_{ji}'', \quad T_{ij}''\,m^{ij\prime} = 0. \end{aligned} \tag{10}$$

In particular, notice that although $\mathbf{T}''$ is a deviatoric tensor its matrix of components T_{ij}'' relative to $\mathbf{m}_i'$ is not a deviatoric matrix since $\mathbf{m}_i'$ are not necessarily orthonormal vectors in nonzero states of stress. However, for metals, $\mathbf{m}_i'$ remain nearly orthonormal.

2.4. Inelastic deformation rate and spin

In (Lee and Rubin, 2020) the direction of the inelastic deformation rate was specified by

$$\bar{\mathbf{D}}_p = \sum_{i=1}^{6} d_i\mathbf{B}_i'', \quad d_1 = 1, \tag{11}$$

where the material constants d_i must be restricted so that the material dissipation inequality is satisfied. Necessary restrictions on the values of d_i where developed which ensure that inelastic deformation rate is dissipative for the small elastic distortional strain approximation. Here, it is noted that since $\mathbf{D}_p = \Gamma\bar{\mathbf{D}}_p$, the function Γ multiplies all of the constants d_i so the constant d_1 can be set equal to unity without loss in generality. Furthermore, since the tensors $\mathbf{B}_i''$ in (7) depend on the microstructural vectors $\mathbf{m}_i'$ and the deviatoric stress $\mathbf{T}''$ in (9) depends on $\mathbf{B}_i''$, the direction of inelastic deformation rate $\bar{\mathbf{D}}_p$ in (11) also depends on the stress through the microstructural vectors $\mathbf{m}_i'$.

In addition, the direction of inelastic spin was specified by

$$\begin{aligned} \bar{\mathbf{W}}_p = {} & \Omega_{12}\left[\bar{\mathbf{D}}_p\cdot(\mathbf{m}_1'\otimes\mathbf{m}_2')\right](\mathbf{m}^{1\prime}\otimes\mathbf{m}^{2\prime} - \mathbf{m}^{2\prime}\otimes\mathbf{m}^{1\prime}) \\ & + \Omega_{31}\left[\bar{\mathbf{D}}_p\cdot(\mathbf{m}_3'\otimes\mathbf{m}_1')\right](\mathbf{m}^{3\prime}\otimes\mathbf{m}^{1\prime} - \mathbf{m}^{1\prime}\otimes\mathbf{m}^{3\prime}) \\ & + \Omega_{23}\left[\bar{\mathbf{D}}_p\cdot(\mathbf{m}_2'\otimes\mathbf{m}_3')\right](\mathbf{m}^{2\prime}\otimes\mathbf{m}^{3\prime} - \mathbf{m}^{3\prime}\otimes\mathbf{m}^{1\prime}), \end{aligned} \tag{12}$$

where Ω_{12}, Ω_{31} and Ω_{23} were material constants and for convenience the indices of Ω_{13} have been reversed. In this paper, this functional form for inelastic spin is modified by specifying the coefficients to be functions

$$\Omega_{12} = \bar{\Omega}_{12}\chi_{12}, \quad \Omega_{31} = \bar{\Omega}_{31}\chi_{31}, \quad \Omega_{23} = \bar{\Omega}_{23}\chi_{23}, \tag{13}$$

where $\bar{\Omega}_{12}, \bar{\Omega}_{31}$ and $\bar{\Omega}_{23}$ are constants, the auxiliary variables χ_{12}, χ_{31} and χ_{23} are specified by

$$\begin{aligned} &\chi_{12} = \tfrac{2}{\pi}\tan^{-1}\left(\tfrac{e_{22}''-e_{11}''}{2e_{12}''}\right), \quad \chi_{31} = \tfrac{2}{\pi}\tan^{-1}\left(\tfrac{e_{11}''-e_{33}''}{2e_{13}''}\right), \\ &\chi_{23} = \tfrac{2}{\pi}\tan^{-1}\left(\tfrac{e_{33}''-e_{22}''}{2e_{23}''}\right), \end{aligned} \tag{14}$$

and the deviatoric elastic distortional strains e_{ij}'' are defined by

$$e_{ij}'' = \frac{1}{2}\left(m_{ij}' - \frac{1}{3}m_{nn}'\delta_{ij}\right). \tag{15}$$

From (11), (12) and (A.1) it can be seen that $\bar{\mathbf{W}}_p$ vanishes when $\mathbf{m}_i'$ are parallel to the principal directions of $\bar{\mathbf{D}}_p$, independently of the functions Ω_{ij}. The function χ_{12} vanishes when $\mathbf{m}_1'$ and $\mathbf{m}_2'$ are nearly aligned with vectors that are averages of the principal directions of the matrix of components of $\bar{\mathbf{D}}_p$ in the $\mathbf{m}_1'$-$\mathbf{m}_2'$ plane, which would again cause the component of $\bar{\mathbf{W}}_p$ in the $\mathbf{m}_1'$-$\mathbf{m}_2'$ plane to vanish. Also, the magnitude of χ_{12} is bounded by unity and has the sign of its argument. It will be seen later that this functional form for χ_{12} allows the proposed model to be calibrated to measured data for the orientation change of the principal directions of inelastic orthotropy for uniaxial stress loadings at angles to the RD. In addition, since a plane stress constitutive equation is used for sheet metal, the values of $\bar{\Omega}_{13}$ and $\bar{\Omega}_{23}$ are set equal to zero

$$\bar{\Omega}_{13} = \bar{\Omega}_{23} = 0. \tag{16}$$

2.5. Yield function and loading conditions

In (Lee and Rubin, 2020) the Coupled Quadratic-Nonquadratic yield function F proposed in (Lee et al., 2017) for sheet metal in terms of stress was reformulated as the yield function g in terms of the elastic dilatation J_e, the microstructural elastic distortional deformation metric m_{ij}' and a non-dimensional hardening variable κ

$$F(T_{ij}, \kappa) = g\left(J_e, m_{ij}', \kappa\right), \tag{17}$$

with κ determined by the evolution equation

$$\dot{\kappa} = \Gamma H, \quad H = \sqrt{\frac{2}{3}\bar{\mathbf{D}}_p\cdot\bar{\mathbf{D}}_p}, \tag{18}$$

which can be identified as an equivalent inelastic deformation rate. Details of this yield function, especially related to the material constants recorded in Tables 2 and 3 introduced later, can be found in (Lee and Rubin, 2020).

To determine the function Γ in (4) and (18) it is convenient to write the material derivatives of the stress components T_{ij} in the forms

$$\dot{T}_{ij} = \mathbf{C}_{ij}\cdot\mathbf{D} - \Gamma\mathbf{R}_{ij}\cdot\bar{\mathbf{D}}_p, \quad \mathbf{C}_{ij} = \frac{\partial T_{ij}}{\partial J_e}J_e\mathbf{I} + \mathbf{R}_{ij}, \quad \mathbf{R}_{ij} = \frac{\partial T_{ij}}{\partial m_{rs}'}\mathbf{M}_{rs}, \tag{19}$$

with $\mathbf{M}_{ij}$ defined in (5). Also, use can be made of the results

$$\frac{\partial m_{ij}'}{\partial m_{rs}'} = \delta_i^r\delta_j^s, \quad \frac{\partial m^{ij\prime}}{\partial m_{rs}'} = -m^{ir\prime}m^{js\prime}, \tag{20}$$

to evaluate the tensors $\mathbf{R}_{ij}$. It then follows that

$$\dot{g} = \hat{g} - \Gamma\overline{g}, \quad \hat{g} = \frac{\partial F}{\partial T_{ij}}\mathbf{C}_{ij}\cdot\mathbf{D}, \quad \overline{g} = \frac{\partial F}{\partial T_{ij}}\mathbf{R}_{ij}\cdot\bar{\mathbf{D}}_p - \frac{\partial F}{\partial\kappa}H, \tag{21}$$

so the loading conditions in strain space [e.g. Naghdi and Trapp (1975)] require

$$\begin{aligned} &\Gamma = 0 \text{ for } g < 0 \quad \text{or} \quad [g = 0, \hat{g} \leqslant 0], \\ &\Gamma = \tfrac{\hat{g}}{\overline{g}} > 0 \quad \text{for} \quad [g = 0, \hat{g} > 0]. \end{aligned} \tag{22}$$

Furthermore, using these expressions the stress rates $\dot{T}_{ij}$ are given by

$$\begin{aligned} &\dot{T}_{ij} = \mathbf{K}_{ij}\cdot\mathbf{D}, \quad \mathbf{K}_{ij} = \mathbf{K}_{ji}, \quad \mathbf{K}_{ij}^T = \mathbf{K}_{ij}, \\ &\mathbf{K}_{ij} = \mathbf{C}_{ij} \quad \text{for} \quad \Gamma = 0, \\ &\mathbf{K}_{ij} = \mathbf{C}_{ij} - \left(\tfrac{\mathbf{R}_{ij}\cdot\bar{\mathbf{D}}_p}{\overline{g}}\right)\tfrac{\partial F}{\partial T_{rs}}\mathbf{C}_{rs} \text{ for} \quad \Gamma > 0. \end{aligned} \tag{23}$$

3. The Lagrangian and Eulerian models used for comparison

The objective of this section is to a specify a Lagrangian model for comparison with the Eulerian model summarized in Section 2.

Table 1
Material properties of AA6022-T4: Data from (Stoughton and Yoon, 2009).

Loading direction	Yield stress [MPa]	R-values	Isotropic elastic properies [GPa]
0°	136	1.029	
15°	137	1.010	
30°	138	0.703	$K = 58.33$
45°	136	0.532	
60°	134	0.553	$\mu = 26.92$
75°	131	0.689	
90°	128	0.728	

Table 2
Parameters in the New model for the CQN yield function Yld2000-2d for AA6022-T4.

Anisotropic yield function parameters						
Loading direction	Hardening parameters					Exponent
	A_θ [MPa]	B_θ [MPa]	C_θ	D_θ	E_θ [MPa]	(n)
0°	333.86	202.29	10.38	1.00	0.42	
45°	335.22	199.10	8.99	1.00	0.38	10
90°	322.13	193.64	9.20	1.00	0	
EB	362.06	233.21	7.35	1.00	2.55	
Anisotropic inelastic parameters						
		d_1	d_2	d_3	d_4	
		1	1.469	1.436	−0.5854	

Table 3
Parameters in the Ref Model for yield function Yld2000-2d model for AA6022-T4.

Yld2000-2d model $(n = 8)$							
α_1	α_2	α_3	α_4	α_5	α_6	α_7	α_8
0.9699	1.0760	1.0339	1.0700	1.0287	1.1312	0.96640	1.0074

Common Lagrangian formulations for sheet metal [e.g., (Chung and Richmond, 1992; Chung and Richmond, 1993; Yoon et al., 1999; Kim and Yang, 2007) do not model inelastic spin. Instead, the principal directions of orthotropic inelastic deformation rate in this model are referred to an evolving orthonormal triad of vectors $\mathbf{n}_i$, which is determined by integrating the evolution equations

$$\dot{\mathbf{n}}_i = \left(\dot{\mathbf{R}}\mathbf{R}^T\right)\mathbf{n}_i, \tag{24}$$

where $\mathbf{R}$ is the rotation tensor defined by the polar representation of the total deformation gradient $\mathbf{F}$. Here, this model with the Yld2000-2d yield function developed in (Barlat et al., 2003) is reference model and is referred to as the *Ref model*.

The second model, developed in (Lee and Rubin, 2020) and reviewed and modified in Section 2, is based on the microstructural vectors $\mathbf{m}_i'$ determined by the evolution Eqs. (4) and employs the CQN yield function developed in (Lee et al., 2017). For convenience this model is referred to here as the *New model* since it uses the new constitutive Eqs. (13) for inelastic spin. It is emphasized that the orientation of the principal directions of inelastic deformation rate are determined naturally by the microstructural vectors $\mathbf{m}_i'$ even though elastic deformation causes the triad $\mathbf{m}_i'$ to become stretched and skewed. Moreover, it will be seen later that the inelastic spin in (12) controls orientation changes of $\mathbf{m}_i'$.

For all of the following examples, the simulations consider AA6022-T4 sheet metal, whose properties are summarized in Table 1. The model parameters for the yield function (CQN model) and the anisotropic inelastic deformation rate are presented in Table 2. The constants d_2, d_3 and d_4 characterizing the orthotropic inelastic deformation rate were determined analytically from the R-values measured for the loading angles $0^\circ, 45^\circ$ and 90° from the *RD*, as explained in (Lee and Rubin, 2020). The other parameters in the CQN yield function were determined by the evolution of strength anisotropy using data for uniaxial stress loading at angles $0^\circ, 45^\circ$ and 90° relative the *RD* and for equibiaxial loading (*EB*). In (Lee and Rubin, 2020), the distortional hardening in the model was verified for four levels of strain (4%, 10%, 20% and 30%).

For the examples in this paper it is sufficient to specify $\bar{\Omega}_{31} = \bar{\Omega}_{23} = 0$ in (13) because the sheet metal model uses a constitutive equation for plane stress. Also, in the initial zero-stress configuration, the initial values of $\mathbf{m}_i'$ and $\mathbf{n}_i$ are specified to coincide

$$\mathbf{m}_i'(0) = \mathbf{n}_i(0) = \mathbf{e}_i, \tag{25}$$

where $\mathbf{e}_i$ is a fixed orthonormal triad with $\mathbf{e}_1$ parallel to the *RD* direction, $\mathbf{e}_2$ parallel to the *TD* direction and $\mathbf{e}_3$ parallel to the thickness direction.

To study differences in the orientations predicted by these two models for the examples of plane strain deformations in the $\mathbf{e}_1$-$\mathbf{e}_2$ plane, it is convenient to define the orientation angles θ_1, θ_2 and θ by the expressions

$$\begin{aligned} &\tfrac{\mathbf{m}_1'}{|\mathbf{m}_1'|} = \cos\theta_1\mathbf{e}_1 + \sin\theta_1\mathbf{e}_2,\ \tfrac{\mathbf{m}_2'}{|\mathbf{m}_2'|} = -\sin\theta_2\mathbf{e}_1 + \cos\theta_2\mathbf{e}_2, \\ &\mathbf{n}_1 = \cos\theta\mathbf{e}_1 + \sin\theta\mathbf{e}_2,\ \mathbf{n}_2 = -\sin\theta\mathbf{e}_1 + \cos\theta\mathbf{e}_2. \end{aligned} \tag{26}$$

Also, Matlab codes were used to predict the response of a single element for the analysis of plane strain problems discussed in Sections 5 and 6.

4. Uniaxial stress response

Simulations were performed for uniaxial stress loading of a single element at angles 0° to 90° from the rolling direction *RD* (with 15° intervals) to validate the model. These simulations used the material parameters for AA6022-T4 recorded in Table 1. The New model uses the parameters recorded in Table 2 and the Ref model uses the parameters recorded in Table 3.

4.1. Calibration of the value of $\bar{\Omega}_{12}$

To calibrate the value of $\bar{\Omega}_{12}$, use is made of the measured data for the rotation angle θ of the orthotropic axes in (Tong et al., 2004). Specifically, the value of this angle was measured for uniaxial stress loading at a range of angles relative to the RD and at the value of inelastic strain $\kappa = 0.2$. Fig. 1 shows that the predictions of the New model for θ_1 and θ_2 using the inelastic spin (12) based on the modified function (13) are in reasonable agreement with the measured data for Ω_{12} calibrated to the value

$$\bar{\Omega}_{12} = 500. \tag{27}$$

In contrast, the rotation tensor for uniaxial tension is given by $\mathbf{R} = \mathbf{I}$ so the Ref model predicts that $\theta = 0$, which is inconsistent with the measured data. Since the elastic deformations in sheet metal remain small, the value of θ_1, which characterizes the direction of $\mathbf{m}_1'$, and the value of θ_2, which characterizes the direction of $\mathbf{m}_2'$ defined in (26) are close to each other. Fig. 1 shows the importance

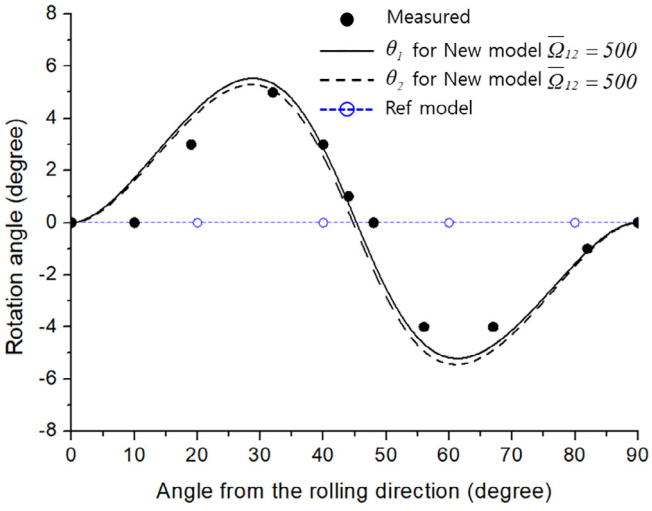

Fig. 1. Calibration of the value $\bar{\Omega}_{12} = 500$ in the New model which shows that predictions of the angles θ_1 and θ_2 are in reasonable agreement with the experimental data for uniaxial stress in (Tong et al., 2004) with $\kappa = 0.2$.

of modeling inelastic spin as suggested in (Dafalias and Rashid, 1989; Kim, 1992; Kim and Yin, 1997; Hill, 1998; Hahm and Kim, 2008).

4.2. Predictions of the stress–strain response and R-value distribution

Fig. 2 shows predictions of the New model [using the specification (27)] together with experimental data from (Stoughton and Yoon, 2009). Fig. 2a shows stress–strain curves for uniaxial stress and EB loadings and Fig. 2b shows the R-value distribution for

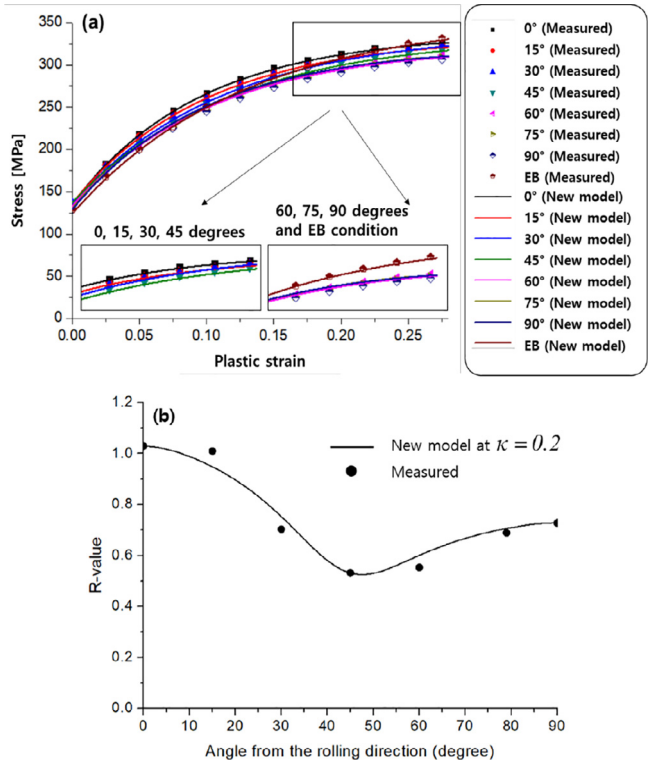

Fig. 2. Predictions of the new model with $\bar{\Omega}_{12} = 500$ compared with measured data (Stoughton and Yoon, 2009): (a) Stress–strain responses for uniaxial stress and EB loadings; and (b) the R-value distribution for uniaxial stress at $\kappa = 0.2$.

$\kappa = 0.2$. From these figures it can be seen that the value $\bar{\Omega}_{12} = 500$ also causes the predictions of the New model to be in good agreement with this experimental data. These results are also consistent with the measured data in (Hahm and Kim, 2008), where it was shown that rotation of the orthotropic axes does not significantly influence the R-value distribution because the distribution of the rotation angle is symmetrical about 45 degree.

5. Large deformation simple shear loading

5.1. Eulerian formulation

For simple shear ($\dot{\gamma} \geqslant 0$), the velocity gradient $\mathbf{L}$ is given by

$$\mathbf{L} = \dot{\gamma}\mathbf{e}_1 \otimes \mathbf{e}_2, \tag{28}$$

where $\dot{\gamma}$ is the shear rate. Also, specifying $J_e = 1$ in the zero-stress initial state and using the fact that simple shear is isochoric, it follows that the solution of (3) requires

$$J_e = 1. \tag{29}$$

Furthermore, the normal component σ and shear component τ of the traction vector applied to the top surface of a block, with unit normal $\mathbf{n} = \mathbf{e}_2$, are defined by

$$\sigma = \mathbf{T} \cdot \mathbf{e}_2 \otimes \mathbf{e}_2, \quad \tau = \mathbf{T} \cdot \mathbf{e}_1 \otimes \mathbf{e}_2. \tag{30}$$

5.2. Lagrangian formulation based on $\mathbf{n}_i$

The total deformation gradient $\mathbf{F}$ from a zero-stress reference configuration and the rotation tensor $\mathbf{R}$ in the polar representation of $\mathbf{F}$ are given by

$$\mathbf{F} = \mathbf{I} + \gamma \mathbf{e}_1 \otimes \mathbf{e}_2,$$
$$\mathbf{R} = \tfrac{1}{\sqrt{4+\gamma^2}}[2(\mathbf{e}_1 \otimes \mathbf{e}_1 + \mathbf{e}_2 \otimes \mathbf{e}_2) + \gamma(\mathbf{e}_1 \otimes \mathbf{e}_2 - \mathbf{e}_2 \otimes \mathbf{e}_1)] + \mathbf{e}_3 \otimes \mathbf{e}_3, \tag{31}$$

where γ is the shear strain from the reference configuration. Now, using (24) and (26), the evolution equation for θ is given by

$$\dot{\theta} = \left(\dot{\mathbf{R}}\mathbf{R}^T\right) \cdot \mathbf{n}_2 \otimes \mathbf{n}_1 = -\frac{2\dot{\gamma}}{4+\gamma^2}, \tag{32}$$

which with the help of the initial conditions (25) can be integrated to obtain

$$\theta = -\tan^{-1}\left(\frac{\gamma}{2}\right). \tag{33}$$

5.3. Unphysical influence of the reference configuration in the Lagrangian formulation

Fig. 3 shows the undeformed ($\gamma = 0$) configuration, which is skewed to the left, the partially deformed configuration ($\gamma = 2.5$), which is a square and the deformed ($\gamma = 5$), which is skewed to the right. This unusual skewed shape in the zero-stress reference configuration is introduced to help interpret the unphysical influence of the reference configuration on the formulation based on $\mathbf{n}_i$.

A fundamental difference between the Eulerian formulation based on J_e and $\mathbf{m}_i'$, recorded in Section 2, and the Lagrangian formulation based on the evolution Eq. (24) for $\mathbf{n}_i$ is that the Eulerian formulation is insensitive to arbitrariness of: a reference configuration; a zero-stress intermediate configuration; a total deformation measure; and an inelastic deformation measure (Rubin, 1996; Rubin, 2001; Rubin, 2012). Specifically, from (33) it is clear that θ and $\mathbf{n}_i$ depend explicitly on the choice of the reference configuration and on the total shear γ from the reference configuration.

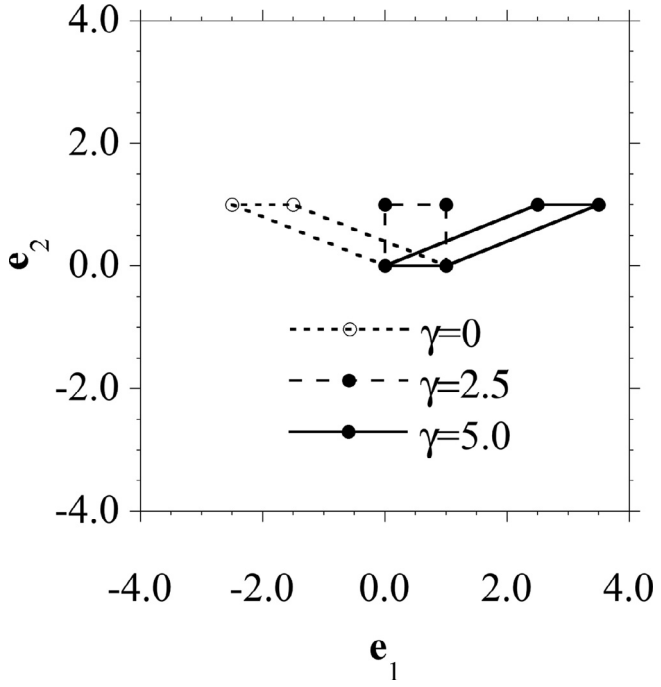

Fig. 3. Simple shear showing the undeformed ($\gamma = 0$), partially deformed ($\gamma = 2.5$) and fully deformed ($\gamma = 5.0$) shapes.

Given knowledge of the material only in its partially deformed state at $\gamma = 2.5$ in Fig. 3, it is not possible to determine the arbitrary choice of the reference configuration or the value of γ from this arbitrary reference configuration. Consequently, γ is not an internal state variable in the sense discussed by Onat (1968). However, the stress state (which determines the elastic deformation measures), the orientations of $\mathbf{n}_i$ and the values of the hardening variables can be determined by experiments on identical samples of the material in its current state, independent of any choice of the reference configuration. In particular, the measured orientations of $\mathbf{n}_i$ determine the value of θ at $\gamma = 2.5$

$$\theta(2.5) = -\tan^{-1}(1.25). \tag{34}$$

As already mentioned, it is not possible to measure the value of γ.

Since the choice of the reference configuration is arbitrary, it should be possible to reset the reference configuration to be the loaded configuration at $\gamma = 2.5$ and define the relative deformation gradient $\mathbf{F}_r$, the relative shear strain γ_r, the relative rotation $\mathbf{R}_r$ and the relative rotation rate $\dot{\theta}_r$ by the expressions

$$\begin{aligned}
&\mathbf{F}_r = \mathbf{I} + \gamma_r \mathbf{e}_1 \otimes \mathbf{e}_2, \quad \dot{\gamma}_r = \dot{\gamma}, \quad \mathbf{L} = \dot{\mathbf{F}}_r \mathbf{F}_r^{-1} = \dot{\gamma} \mathbf{e}_1 \otimes \mathbf{e}_2, \\
&\mathbf{R}_r = \tfrac{1}{\sqrt{4+\gamma_r^2}} [2(\mathbf{e}_1 \otimes \mathbf{e}_1 + \mathbf{e}_2 \otimes \mathbf{e}_2) + \gamma_r (\mathbf{e}_1 \otimes \mathbf{e}_2 - \mathbf{e}_2 \otimes \mathbf{e}_1)] + \mathbf{e}_3 \otimes \mathbf{e}_3, \\
&\dot{\theta}_r = -\tfrac{\dot{\gamma}_r}{4+\gamma_r^2}.
\end{aligned} \tag{35}$$

Then, integrating the evolution for θ_r subject to the value (34) yields

$$\begin{aligned}
&\theta_r = -\tan^{-1}(1.25) - \tan^{-1}\left(\tfrac{\gamma_r}{2}\right) \text{for} \quad \gamma_r \geqslant 0, \\
&\gamma_r = \gamma - 2.5.
\end{aligned} \tag{36}$$

Fig. 4 compares the orientation angle θ of $\mathbf{n}_i$ in (33) based on the reference configuration at $\gamma = 0$ with the angle θ_r in (36) determined by resetting the reference configuration at $\gamma = 2.5$. Since θ_r does not follow the same curve as θ after changing the reference configuration at $\gamma = 2.5$, this figure clearly shows the significant unphysical influence of the choice of the reference configuration on the Lagrangian formulation based on $\mathbf{n}_i$. In contrast, the evolution equations for $\mathbf{m}_i'$ in the Eulerian model discussed here are determined by the evolution Eqs. (4) with the function χ_{12} in (13). These evolution equations depend on the current state of the material and on the current velocity gradient, which are uninfluenced by any choice of the reference configuration.

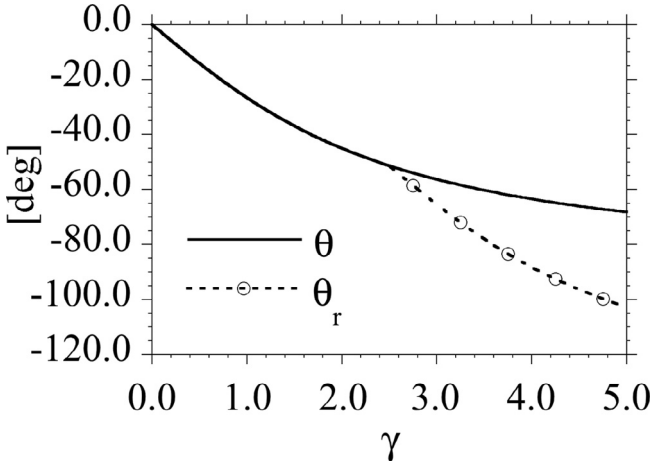

Fig. 4. Simple shear: Comparison of the orientation angle θ of $\mathbf{n}_i$ for the reference configuration defined by $\gamma = 0$ and the orientation angle θ_r associated with resetting the reference configuration at $\gamma = 2.5$.

5.4. Parameter study of $\bar{\Omega}_{12}$ for large deformation simple shear

Fig. 5 shows predictions of the rotation angle θ_1 (Fig. 5a), the normal stress σ (Fig. 5a), and the shear stress τ (Fig. 5c) for different increasing values of $\bar{\Omega}_{12}$. Fig. 6 shows similar plots for different decreasing values of $\bar{\Omega}_{12}$. From these figures it can be seen that τ is uninfluenced by the value of $\bar{\Omega}_{12}$ but the values of θ_1 and σ are significantly influenced by its value. In this regard, it is recalled that the value $\bar{\Omega}_{12} = 500$ was calibrated relative to the measured data in Fig. 1. Also, it is observed from Fig. 5a that θ_1 tends to asymptotically approach the value of $\theta_1 = 45^\circ$ for large positive values of $\bar{\Omega}_{12}$ and from Fig. 6a that θ_1 tends to asymptotically approach the value of $\theta_1 = 0^\circ$ for large negative values of $\bar{\Omega}_{12}$.

From the results in Figs. 5 and 6, it is not clear if positive or negative values of $\bar{\Omega}_{12}$ are more physical. Fig. 1 shows that the positive value $\bar{\Omega}_{12} = 500$ predicts the measured data for uniaxial stress in (Tong et al., 2004) with $\kappa = 0.2$. However, Fig. 7 shows that the negative value $\bar{\Omega}_{12} = -500$ predicts the opposite trend to the data.

Furthermore, Fig. 8 considers large deformation simple shear and compares the orientation angle θ_1 predicted by the New model with $\bar{\Omega}_{12} = 0, 500$, and the orientation angle θ in (33) predicted by the Ref model with the reference configuration defined by $\gamma = 0$ and predicted by the ε^{sim} strain path model in (Barlat et al., 1993), which is another Lagrangian model. As discussed in (Barlat et al., 1993), the ε^{sim} strain path model predicts excessive rotation of the orthotropic axes. From Fig. 8 it can be seen that θ_1 predicted by the New model with no inelastic spin ($\bar{\Omega}_{12} = 0$) is the same as θ predicted by the ε^{sim} strain path model. Although the value of θ_1 predicted by the New model with $\bar{\Omega}_{12} = 500$ is similar to the value of θ predicted by the Ref model, this value of $\bar{\Omega}_{12}$ has been calibrated to match the measured rotation for uniaxial stress in (Tong et al., 2004). Moreover, it is recalled that, in contrast with the Eulerian formulation of the New model, the Lagrangian formulation of the Ref model exhibits unphysical dependence on the reference configuration.

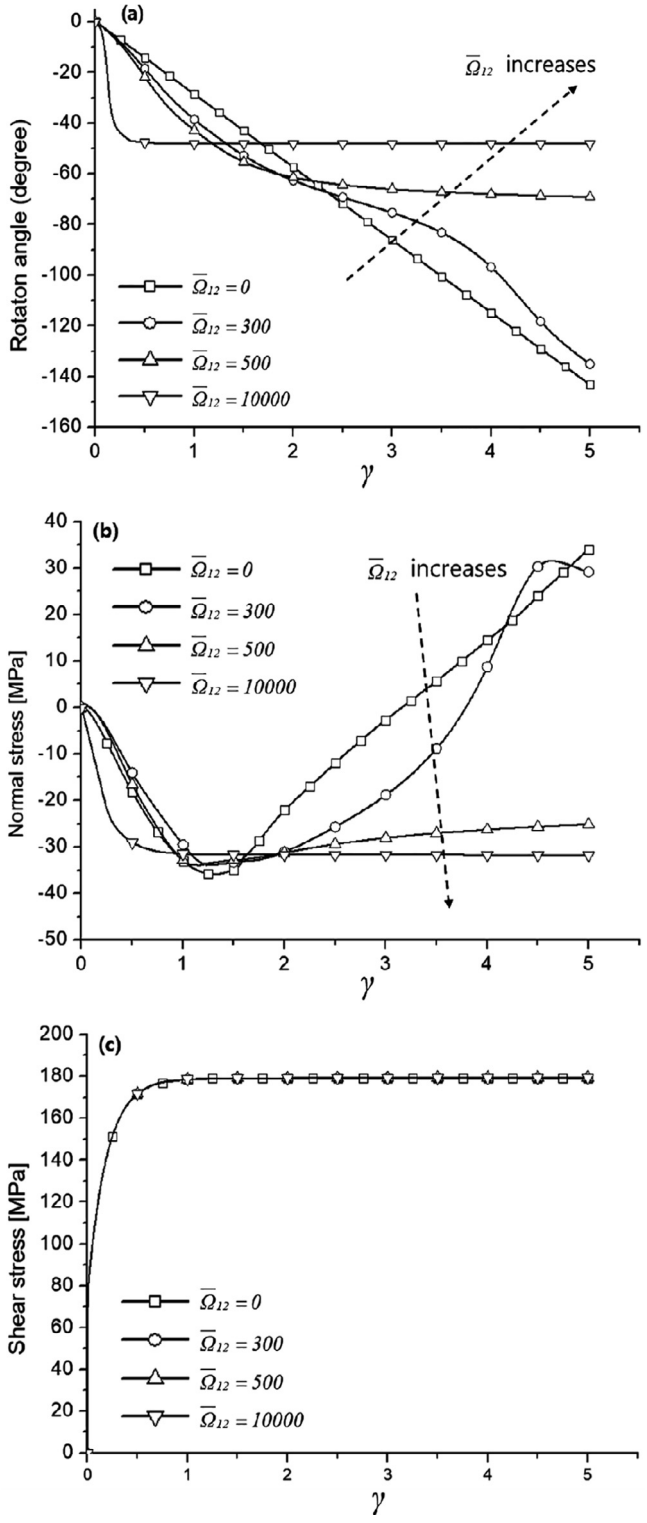

Fig. 5. Simple shear: Influence of increasing values of $\bar{\Omega}_{12}$ on: (a) the rotation angle θ_1; (b) the normal stress σ; and (c) the shear stress τ.

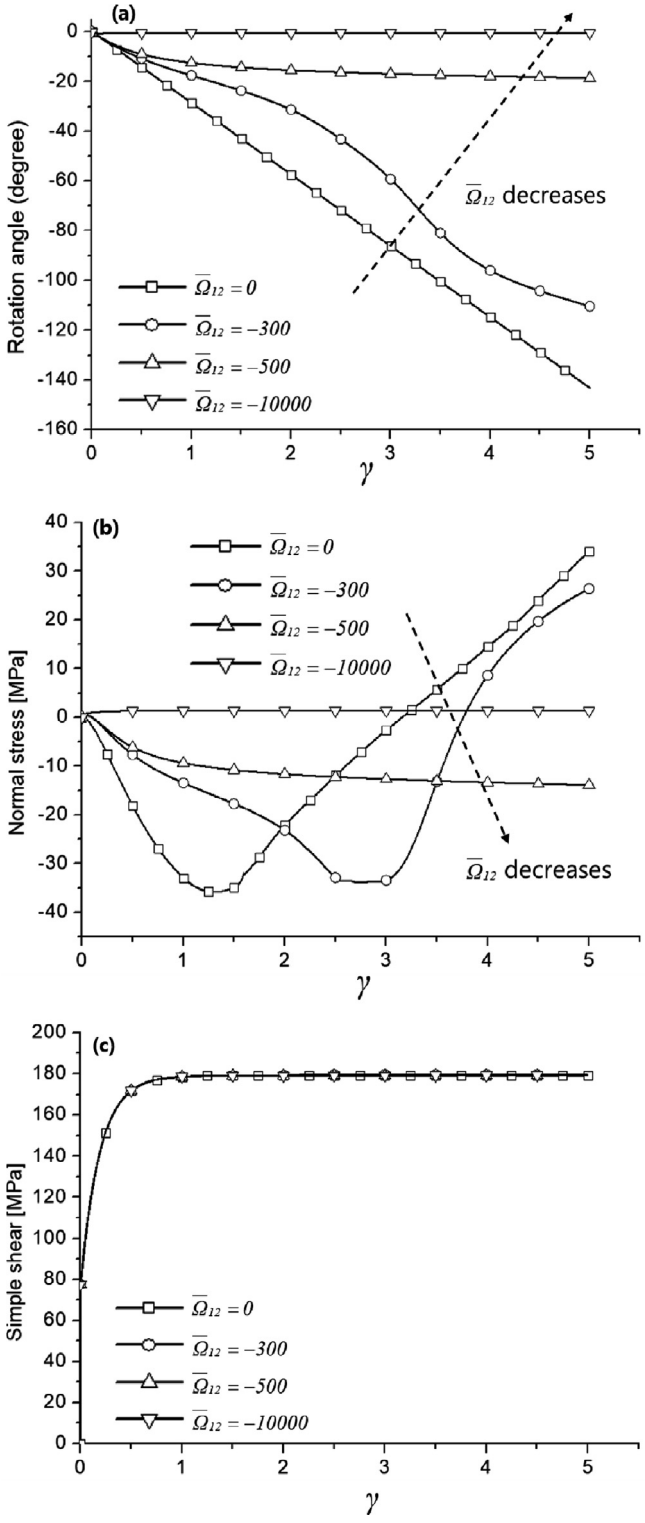

Fig. 6. Simple shear: Influence of decreasing values of $\bar{\Omega}_{12}$ on: (a) the rotation angle θ_1; (b) the normal stress σ; and (c) the shear stress τ.

6. Conclusions

Using the developments in (Lee and Rubin, 2020) and the new functional forms (13) for inelastic spin proposed in this paper, the Eulerian formulation based on the evolution of the microstructural vectors $\mathbf{m}_i'$ has been shown to predict results that are in good agreement with measured data for AA6022-T4. Specifically, the New model predicts the stress–strain response to uniaxial stress at angles relative to the RD and for equibiaxial loading as well as the R-value distribution. Also, the new material constant $\bar{\Omega}_{12}$, which controls inelastic spin, has been calibrated to predict good agreement with measured data for the rotation angle θ_1 for uniaxial stress loading at angles relative to the RD.

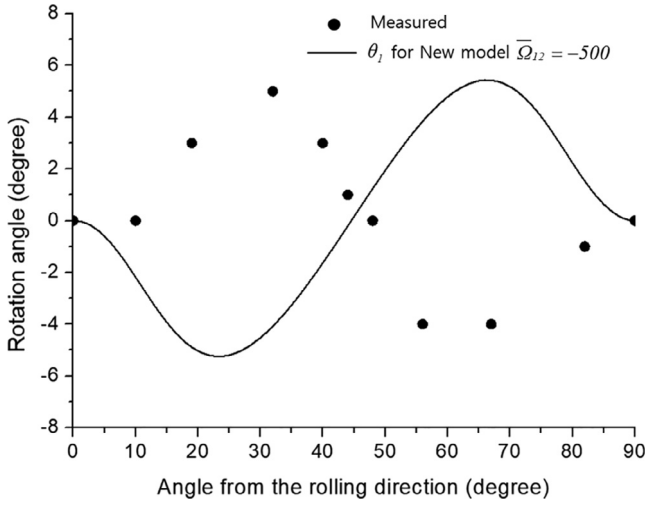

Fig. 7. Predictions of θ_1 for $\bar{\Omega}_{12} = -500$ together with measured data for uniaxial stress in (Tong et al., 2004) with. $\kappa = 0.2$.

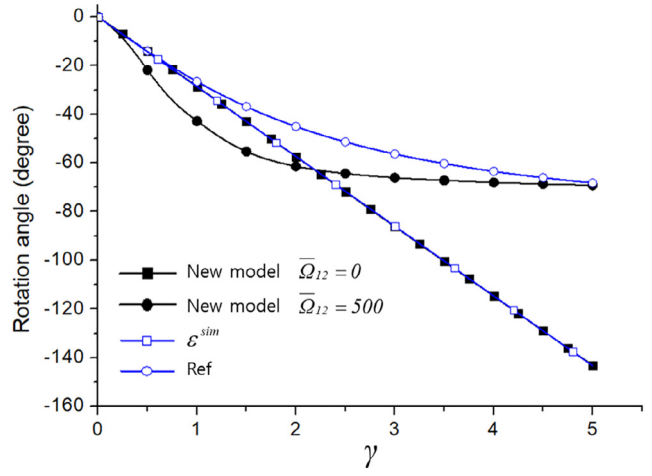

Fig. 8. Simple shear: Comparison of the orientation angle θ_1 predicted by the Eulerian formulation of the New model and the orientation angle θ predicted by the Lagrangian formulations of the Ref model and the ε^{sim} strain model in (Barlat et al., 1993).

In addition, it has been shown that a common Lagrangian formulation which determines the orientation of the axes of inelastic orthotropy based on the rotation tensor in the polar representation of the total deformation gradient exhibits unphysical dependence on the reference configuration. In contrast, the Eulerian formulation based on the microstructural vectors is insensitive to arbitrariness of a reference configuration.

Declaration of Competing Interest

The authors declare that they have no known competing financial interests or personal relationships that could have appeared to influence the work reported in this paper.

Acknowledgements

EH Lee acknowledges partial support from the National Research Foundation of Korea (NRF) grant (No. 2020R1F1A1069535) funded by the Korea government.

Appendix A. Details of some tensors

The tensors $\mathbf{B}_i''$ in (7) are given by

$$\begin{aligned}
\mathbf{B}_1'' &= \left[\mathbf{m}_1' \otimes \mathbf{m}_1' - \mathbf{m}^{1\prime} \otimes \mathbf{m}^{1\prime} - \tfrac{1}{3}\left(m_{11}' - m^{11\prime}\right)\mathbf{I}\right],\\
\mathbf{B}_2'' &= \left[\mathbf{m}_2' \otimes \mathbf{m}_2' - \mathbf{m}^{2\prime} \otimes \mathbf{m}^{2\prime} - \tfrac{1}{3}\left(m_{22}' - m^{22\prime}\right)\mathbf{I}\right],\\
\mathbf{B}_3'' &= \left[\mathbf{m}_3' \otimes \mathbf{m}_3' - \mathbf{m}^{3\prime} \otimes \mathbf{m}^{3\prime} - \tfrac{1}{3}\left(m_{33}' - m^{33\prime}\right)\mathbf{I}\right],\\
\mathbf{B}_4'' &= \tfrac{m_{12}'}{m_{11}'m_{22}'}\left[\left(\mathbf{m}_1' \otimes \mathbf{m}_2' + \mathbf{m}_2' \otimes \mathbf{m}_1'\right) - \tfrac{m_{12}'}{m_{11}'}\left(\mathbf{m}_1' \otimes \mathbf{m}_1'\right) - \tfrac{m_{12}'}{m_{22}'}\left(\mathbf{m}_2' \otimes \mathbf{m}_2'\right)\right],\\
\mathbf{B}_5'' &= \tfrac{m_{13}'}{m_{11}'m_{33}'}\left[\left(\mathbf{m}_1' \otimes \mathbf{m}_3' + \mathbf{m}_3' \otimes \mathbf{m}_1'\right) - \tfrac{m_{13}'}{m_{11}'}\left(\mathbf{m}_1' \otimes \mathbf{m}_1'\right) - \tfrac{m_{13}'}{m_{33}'}\left(\mathbf{m}_3' \otimes \mathbf{m}_3'\right)\right],\\
\mathbf{B}_6'' &= \tfrac{m_{23}'}{m_{22}'m_{33}'}\left[\left(\mathbf{m}_2' \otimes \mathbf{m}_3' + \mathbf{m}_3' \otimes \mathbf{m}_2'\right) - \tfrac{m_{23}'}{m_{22}'}\left(\mathbf{m}_2' \otimes \mathbf{m}_2'\right) - \tfrac{m_{23}'}{m_{33}'}\left(\mathbf{m}_3' \otimes \mathbf{m}_3'\right)\right].
\end{aligned} \tag{A.1}$$

References

Banabic, D., Aretz, H., Comsa, D.S., Paraianu, L., 2005. An improved analytical description of orthotropy in metallic sheets. Int. J. Plast. 21 (3), 493–512.

Barlat, F., Brem, J.C., Yoon, J.W., Chung, K., Dick, R.E., Lege, D.J., Pourboghrat, F., Choi, S.H., Chu, E., 2003. Plane stress yield function for aluminum alloy sheets – Part 1: Theory. Int. J. Plast. 19 (9), 1297–1319.

Barlat, F., Chung, K., Richmond, O., 1993. Strain rate potential for metals and its application to minimum plastic work path calculations. Int. J. Plast. 9, 51–63.

Barlat, F., Lege, D.J., Brem, J.C., 1991. A six-component yield function for anisotropic materials. Int. J. Plast. 7 (7), 693–712.

Barlat, F., Maeda, Y., Chung, K., Yanagawa, M., Brem, J.C., Hayashida, Y., Lege, D.J., Matsui, K., Murtha, S.J., Hattori, S., et al., 1997. Yield function development for aluminum alloy sheets. J. Mech. Phys. Solids 45 (11–12), 1727–1763.

Batoz, J.L., Guo, Y.Q., Durouz, P., Detraux, J.K., 1989. In: An effective algorithm to estimate the large strains in deep drawing In: Proc. 3rd International Conf. on Industrial Forming Processes (NUMIFORN'89). Balkema Rotterdam, The Netherlands, p. 383.

Bilby B A, Gardner L R T, S.A.N., 1957. Continuous distributions of dislocations and the theory of plasticity. In: Proceedings of the 9th International Congress of Applied Mechanics. University de Brussels 9, 35–44. .

Budiansky, B., 1959. A reassessment of deformation theories of plasticity. J. Appl. Mech. 26, 259–264.

Bunge, H., Nielsen, I., 1997. Experimental determination of plastic spin in polycrystalline materials. Int. J. Plast. 13, 435–446.

Chung, K., Lee, D., 1984. Computer-aided analysis of sheet material forming processes. Advanced Technology of Plasticity 1, 660–665.

Chung, K., Richmond, O., 1992. Ideal forming – I. homogeneous deformation with minimum plastic work. Int. J. Mech. Sci. 34 (7), 575–591.

Chung, K., Richmond, O., 1993. A deformation theory of plasticity based on minimum work paths. Int. J. Plast. 9 (8), 907–920.

Dafalias, Y.F., 1998. Plastic spin: necessity or redundancy? Int. J. Plast. 14, 909–931.

Dafalias, Y.F., Rashid, M.M., 1989. The effect of plastic spin on anisotropic material behavior. Int. J. Plast. 5 (3), 227–246.

Eckart, C., 1948. The thermodynamics of irreversible processes. IV. the theory of elasticity and anelasticity. Phys. Rev. 73, 373–382.

Hahm, J.H., Kim, K.H., 2008. Anisotropic work hardening of steel sheets under plane stress. Int. J. Plast. 24 (7), 1097–1127.

Hill, R., 1948. A theory of the yielding and plastic flow of anisotropic metals. Proceedings of the Royal Society of London. Series A. Mathematical and Physical Sciences 193 (1033), 281–297. .

Hill, R., 1957. Stability of rigid-plastic solids. J. Mech. Phys. Solids 6, 1–8.

Hill, R., 1986. Extremal paths of plastic work and deformation. J. Mech. Phys. Solids 34 (5), 511–523.

Hill, R., 1998. The mathematical theory of plasticity, Vol. 11. Oxford University Press.

Hu, Q., Li, X., Han, X., Li, H., Chen, J., 2017. A normalized stress invariant-based yield criterion: Modeling and validation. Int. J. Plast. 99, 248–273.

Hutchinson, J.W., 1974. Plastic buckling. In: Advances in applied mechanics Elsevier Vol. 14, 67–144.

Kim, J.B., Yoon, J.W., Yang, D.Y., 2000. Wrinkling initiation and growth in modified yoshida buckling test: finite element analysis and experimental comparison. Int. J. Mech. Sci. 42 (9), 1683–1714.

Kim, K.H., 1992. Evolution of anisotropy during twisting of cold drawn tubes. J. Mech. Phys. Solids 40, 127–139.

Kim, K.H., Yin, J.J., 1997. Evolution of anisotropy under plane stress. J. Mech. Phys. Solids 45, 841–8519.

Kim, T.J., Yang, D.Y., 2007. Fe-analysis of sheet metal forming processes using continuous contact treatment. Int. J. Plast. 23 (3), 544–560.

Kröner, E., 1959. General continuum theory of dislocations and intrinsic stresses. Arch. Ration. Mech. Anal. 4, 273–334.

Lee, E.H., 1969. Elastic-plastic deformation at finite strains. J. Appl. Mech. 36, 1–6.

Lee, E.H., Rubin, M.B., 2020. Modeling anisotropic inelastic effects in sheet metal forming using microstructural vectors – Part I: Theory. Int. J. Plast. 134, 102783.

Lee, E.H., Stoughton, T.B., Yoon, J.W., 2017. A yield criterion through coupling of quadratic and non-quadratic functions for anisotropic hardening with non-associated flow rule. Int. J. Plast. 99, 120–143.

Lee, E.H., Yang, D.Y., Yoon, J.W., Yang, W.H., 2015. Numerical modeling and analysis for forming process of dual-phase 980 steel exposed to infrared local heating. Int. J. Solids Struct. 75, 211–224.
Lee, E.H., Yang, D.Y., Yoon, J.W., Yang, W.H., 2017. A manufacturing process using the infrared ray local heating method for seat cross members. The International Journal of Advanced Manufacturing Technology 89 (9–12), 3299–3305.
Leonov, A.I., 1976. Nonequilibrium thermodynamics and rheology of viscoelastic polymer media. Rheologica acta 15, 85–98.
Levy, S., Shih, C.F., Wilkinson, J.P.D., Stine, P., McWilson, R.C., 1978. Analysis of sheet metal forming to axisymmetric shapes. In: Formability Topics-Metallic Materials. ASTM International.
Lou, Y., Yoon, J.W., 2018. Anisotropic yield function based on stress invariants for bcc and fcc metals and its extension to ductile fracture criterion. Int. J. Plast. 101, 125–155.
Nádai, A., Hodge, P.G., 1963. Theory of flow and fracture of solids, vol. ii. J. Appl. Mech. 30, 640.
Naghdi, P.M., Trapp, J.A., 1975. The significance of formulating plasticity theory with reference to loading surfaces in strain space. Int. J. Eng. Sci. 13, 785–797.
Neale, K.W., 1989. Numerical analysis of sheet metal wrinkling. Numiform'89, Thompson et al. (Eds.), 501–505. .
Onat, E.T., 1968. The notion of state and its implications in thermodynamics of inelastic solids. In: Irreversible aspects of continuum mechanics and transfer of physical characteristics in moving fluids. Springer, pp. 292–314.
Park, S.H., Yoon, J.W., Yang, D.Y., Kim, Y.H., 1999. Optimum blank design in sheet metal forming by the deformation path iteration method. Int. J. Mech. Sci. 41 (10), 1217–1232.
Ponter, A.R.S., Martin, J.B., 1972. Some extremal properties and energy theorems for inelastic materials and their relationship to the deformation theory of plasticity. J. Mech. Phys. Solids 20 (5), 281–300.
Rubin, M.B., 1994. Plasticity theory formulated in terms of physically based microstructural variables – Part I. Theory. Int. J. Solids Struct. 31, 2615–2634.
Rubin, M.B., 1996. On the treatment of elastic deformation in finite elastic-viscoplastic theory. Int. J. Plasticity 12, 951–965.
Rubin, M.B., 2001. Physical reasons for abandoning plastic deformation measures in plasticity and viscoplasticity theory. Archives of Mechanics 53, 519–539.
Rubin, M.B., 2012. Removal of unphysical arbitrariness in constitutive equations for elastically anisotropic nonlinear elastic–viscoplastic solids. Int. J. Eng. Sci. 53, 38–45.
Rubin, M.B., 2019. A new approach to modeling the thermomechanical, orthotropic, elastic-inelastic response of soft materials. Mech. Soft Mater. 1, 3. https://doi.org/10.1007/s42558-018-0003-8.
Sklad, M.P., 1986. The numerical analysis of the influence of the material hardening behavior on strain distribution in drawing a sheet metal part of complex shape. In: Proceedings of the Congress International Deep Drawing Research Group, pp. 464–468.
Stören, S., Rice, J.R., 1975. Localized necking in thin sheets. J. Mech. Phys. Solids 23 (6), 421–441.
Stoughton, T.B., Yoon, J.W., 2009. Anisotropic hardening and non-associated flow in proportional loading of sheet metals. Int. J. Plast. 25 (9), 1777–1817.
Tong, W., Tao, H., Jiang, X., 2004. Modeling the rotation of orthotropic axes of sheet metals subjected to off-axis uniaxial tension. J. Appl. Mech. 71, 521–531.
Vladimirov, I.N., Pietryga, M.P., Reese, S., 2010. Anisotropic finite elastoplasticity with nonlinear kinematic and isotropic hardening and application to sheet metal forming. Int. J. Plast. 26 (9), 659–687.
Yoon, J.W., Yang, D.Y., Chung, K., Barlat, F., 1999. A general elasto-plastic finite element formulation based on incremental deformation theory for planar anisotropy and its application to sheet metal forming. Int. J. Plast. 15 (1), 35–67.